Biogeosciences

Supporting Information for

Spatiotemporal patterns in CO_2 fluxes and geochemical weathering in mountain glacial rivers

Jessica A. Serbu[1,2] (ORCID 0000-0002-0109-4550),
Suzanne E. Tank[1] (ORCID 0000-0002-5371-6577),
Bernhard Peucker-Ehrenbrink[2] (ORCID 0000-0002-3819-992X),
Xiying Sun[3]
Craig A. Emmerton[1] (ORCID 0000-0001-9511-9191)
Vincent L. St.Louis[1] (ORCID 0000-0001-5405-1522)

[1]Department of Biological Sciences, University of Alberta, Edmonton, AB, Canada
[2]Marine Chemistry and Geochemistry Department, Woods Hole Oceanographic Institution, Woods Hole, MA, USA
[3]Department of Oceanography, Texas A&M University, College Station, TX, USA

Corresponding author: Jessica Serbu (serbu@ualberta.ca)

Contents of this file:

Introduction

The supporting information enclosed within consists of:

Text S1 – The details of the **inorganic-organic carbon mass balance model** used in this study;

Figures S1 to S9 – A geologic column of our study region (**Figure S1**), discharge for our study sites (**Figure S2**), linear relationships for the interpolation of missing cation data (**Figure S3**), the power relationship between discharge and velocity (**Figure S4**), XRD results (**Figure S5**), Ca/Na versus Mg/Na mixing diagrams (**Figure S6**), patterns in $^{87}Sr/^{86}Sr$ (**Figure S7**), $\delta^{13}C$ (‰) signatures (**Figure S8**), and MEANDIR R vs. Z color-coded by season (**Figure S9**);

Tables S1 to S6 – Sampling site information (**Table S1**), watershed area covered by land class (**Table S2**), hydrometric gauging stations used within the study (**Table S3**), sampling sites binned by season (**Table S4**), MEANDIR endmember statistics (**Table S5**), relative TDS proportions (**Table S6**), and MEANDIR R and Z statistics (**Table S7**); and

References.

Text S1. Inorganic-organic carbon mass balance model

For the full list of the steps and assumptions of the mass balances used to estimate an overall inorganic-organic carbon mass balance, please see Voss et al., 2023.

Step 1: Non-sea salt concentrations (denoted by $Parameter_{nss}$) were first calculated via Cl^- corrected ratios. Sea salt ratios originally published by Gaillardet et al., 1999 and used by Voss et al., 2023 included $Ca^{2+}/Cl^- = 0.017$, $Mg^{2+}/Cl^- = 0.0019$, $Na^+/Cl^- = 0.870$, and $HCO_3^-/Cl^- = 0.000008$ (where DIC was substituted for HCO_3^-). In three cases, sea salt corrected Na^+ resulted in marginally negative values (-0.42, -0.60, -2.00 μM) so these sites were removed from molar ratios involving Na^+.

Step 2: The fraction of riverine DIC from every source but carbonate weathering ($F_{non\text{-}carb}$) was calculated for each sample using a carbonate endmember (carbEM) determined by mixing diagrams of molar concentrations of Ca_{nss}/Na_{nss} versus Mg_{nss}/Na_{nss} (**Figure S6**). We use the Ca^{2+}_{nss}/Na^+_{nss} carbEM and silicate endmembers (silEM) determined in the present study instead of those from the literature (e.g., Gaillardet et al., 1999) because our ratios indicated a large range in high values. Ca^{2+}_{nss}/Na^+_{nss} molar ratios ranged from 8.2 to 678 and Mg^{2+}_{nss}/Na^+_{nss} molar ratios ranged from 5.5 to 405, with values never deviating far from the line of best fit (**Figure S6**). Higher molar ratios are indicative of carbonate weathering as Na^+_{nss} is not produced with carbonate weathering (Millot et al., 2002), whereas values positioning along the line of best fit suggests a close adherence to a two endmember system. Generally, the most downriver sites along each river had relatively lower molar ratios, whereas sites closer to their source glacier had relatively higher molar ratios (**Figure S6A**), suggesting that carbonate weathering dominated in glacier forefields, but silicate weathering increased with distance downriver.

To aid in defining the most appropriate carbonate and silicate endmembers in our system for a mass balance of DIC sources, $^{87}Sr/^{86}Sr$ values from each river aligning with the lowest and highest Ca^{2+}_{nss}/Na^+_{nss} and Mg^{2+}_{nss}/Na^+_{nss} molar ratios were quantified (n=8). However, we ultimately decided that $^{87}Sr/^{86}Sr$ ratios were not suitable to use as endmembers for the mass balance of DIC because our study region did not have lithological contrast like some regions (e.g., Muñoz et al.,

2024). The largest ranges of $Ca^{2+}_{nss}/Na^{+}_{nss}$ and $Mg^{2+}_{nss}/Na^{+}_{nss}$ molar ratios occurred in the spring and autumn shoulder seasons (**Figure S6B**). In spring, snowmelt drives the hydrology of glacial systems (**Figure S2**) (Marshall et al., 2011), and the resultant large volumes of water traversing watersheds can access new pools of solutes such as fresh glacial sediment (Deuerling et al., 2018; St. Pierre et al., 2019). The two highest $Ca^{2+}_{nss}/Na^{+}_{nss}$ and $Mg^{2+}_{nss}/Na^{+}_{nss}$ molar ratios were from spring 2020 when we sampled during torrential rains (Serbu, St.Louis, et al., 2024). High discharge resulted in breached river channels, and along the NSR, flowed across glacial outwash plains, increasing the turbidity and solute loads by possibly resuspending recently deposited glacial sediment (Serbu, St.Louis, et al., 2024). Thus, the two most extreme spring $Ca^{2+}_{nss}/Na^{+}_{nss}$ and $Mg^{2+}_{nss}/Na^{+}_{nss}$ molar ratios (**Figure S6B**) were removed from consideration for endmember compositions for the mass balance of DIC sources.

$$f_{non-carb} = \frac{DIC_{measured} - \left(\frac{Ca_{nss} + Mg_{nss}}{Na_{nss}}\right) x \left(\frac{DIC_{nss\ (carbEM)}}{(Ca_{nss\ (carbEM)} + Mg_{nss\ (carbEM)})/Na_{nss\ (carbEM)}}\right)}{DIC_{measured}}$$

The fraction of riverine DIC sourced from carbonate weathering (f_{carb}) was thus:

$$f_{carb} = 1 - f_{non-carb}$$

Step 3: To calculate the fraction of sulfuric acid (H_2SO_4) involved in weathering reactions (F_{SA}), we followed Voss et al., 2023 who used the estimate of f_{SA} = 0.08 from Spence & Telmer, 2005.

The fraction of carbonic acid (H_2CO_3) driving weathering reactions (f_{CA}) remained:

$$f_{CA} = 1 - f_{SA}$$

Step 4: The fraction of the stable isotope of carbon sourced from carbonate weathering ($\delta^{13}C_{carb}$), non-carbonate weathering ($\delta^{13}C_{non\text{-}carb}$), and organic carbon respiration ($\delta^{13}C_{OC}$) were calculated as follows:

$$\delta C_{carb} = (f_{SA}\ x\ \delta C_{carbEM}) + (f_{SA}\ x\ \ \delta C_{silEM})$$

$$\delta C_{non-carb} = \frac{\delta DI^{13}C\ -\ (f_{carb}\ x\ \delta C_{carb})}{f_{non-carb}}$$

$$\delta C_{OC} = \delta DO^{13}C\ + \delta^{13}C_{fractionation}$$

Where $\delta^{13}C_{fractionation}$ refers to the fractionation of atmospheric $CO_{2(g)}$ transmuting to riverine $HCO_3^-{}_{(aq)}$, or 9.6 as calculated by Voss et al., 2023.

Step 5: The fraction of riverine DIC from silicate weathering or OC respiration (f_{sil+OC}) was calculated as:

$$f_{sil+OC} = \frac{\delta C_{non-carb} - (\delta^{13}C_{CO_2(atm)} + \delta^{13}C_{fractionation})}{\delta C_{OC} - (\delta^{13}C_{CO_2(atm)} + \delta^{13}C_{fractionation})}$$

Where $\delta^{13}C_{CO_2(atm)}$ refers to the stable isotope of atmospheric CO_2, or -7.25 as determined by Marwick et al., 2015. The fraction of riverine DIC sourced from the atmosphere (f_{atm}) was thus:

$$f_{atm} = 1 -\ f_{sil+OC}$$

Step 6: The fraction of riverine DIC from silicates alone (f_{sil}) was calculated using the sample, carbonate endmember, and silicate endmember $Ca^{2+}{}_{nss}/Na^{+}{}_{nss}$.

$$f_{sil} = \left(\frac{\left(\frac{Ca_{nss}}{Na_{nss}}\right) - \left(\frac{Ca_{nss\ (carbEM)}}{Na_{nss\ (carbEM)}}\right)}{\left(\frac{Ca_{nss\ (silEM)}}{Na_{nss\ (silEM)}}\right) - \left(\frac{Ca_{nss\ (carbEM)}}{Na_{nss\ (carbEM)}}\right)} \right)$$

F_{sil} was then used to calculate the concentration of Na^+ and HCO_3^- that were derived from silicates (ion_{sil}) and non-silicates ($ion_{non\text{-}sil}$):

$$Na_{sil} = f_{sil}\ x\ Na_{nss}$$

$$Na_{non-sil} = Na_{nss} - Na_{sil}$$

$$HCO_{3\ sil} = HCO_{3\ nss\ (silEM)}\ x\ Na_{sil}$$

$$HCO_{3\ non-sil} = HCO_{3\ nss\ (carbEM)}\ x\ Na_{non-sil}$$

Step 7: Finally, the concentrations of DIC from carbonate weathering and atmospheric $CO_{2(g)}$ ($DIC_{carb+atm}$), silicate weathering (DIC_{sil}), and OC respiration (DIC_{OC}) were calculated as:

$$DIC_{sil} = HCO_{3\ sil}$$

$$DIC_{OC} = (f_{sil+OC}\ x\ f_{non-carb}\ x\ DIC) - DIC_{sil}$$

$$DIC_{carb+atm} = DIC - DIC_{sil} - DIC_{OC}$$

DIC concentrations were then converted into percentages for data analysis. On the few occasions the model estimated percent values of DIC from various sources below 0% or slightly above 100%, those data were set to 0% and 100%, respectively, for ease of interpretation.

Geochronologic unit			Chronostratigraphic unit
Cenozoic Era 66 mya to today	Neogene	Holocene & Pleistocene	Glacial deposits (N)
		Pliocene	Pre-glacial gravel (N)
		Miocene	Cave silts (N)
	Paleogene	Oligocene	
		Eocene	
		Paleocene	Paskapoo (N) – ss, sh
Mesozoic Era 252 mya to 66 mya	Cretaceous	Upper	Brazeau (N) – ss, sh Alberta (M) – sh, ss
		Lower	Luscar (N/M) – ss, sh, col Blairmore (N) – ss, sh Cadomin (N) - cgl
	Jurassic	Upper	Fernie (M) – sh, slt, ss
		Middle	
		Lower	
	Triassic	Upper	Spray River (M) – slt, slty dol
		Middle	
		Lower	
Paleozoic Era 541 mya to 252 mya	Permian	Upper	
		Lower	Ishbel – silty dol, chrt, pho
	Carboniferous	Upper	Spray Lakes – dol, slt, ss
		Lower	Rundle – ls, dol Banff – slty dol, sh, ls
	Devonian	Upper	Exshaw – sh Palliser – ls, dol Sassenach – slty dol Fairholme – dol, sh, ls
		Middle	Golden Embayment – ls, dol, ss, gyp
		Lower	
	Silurian	Upper	
		Lower	Tegart – shly ls
	Ordovician	Upper	Beaverfoot – dol, ls Mount Wilson – qtz
		Middle	Owen Creek – dol, sh, ss Skoki – dol
		Lower	Tipperary – qtz Outram – ls, sh, slt Survey Peak – sh, ls, slt
	Cambrian	Upper	Lynx – dol, ls, slt, ss Mistaya – ls Bison Creek – ls, sh Lyell/Ottertail – ls, dol, slt Sullivan – sh, ls, slt
		Middle	Waterfowl – dol, ls Arctomys – sh, slt Pika – ls, dol Eldon – ls, dol Stephen – sh Cathedral – dol, ls, sh Mount Whyte – sh, ls, slt, ss
		Lower	Gog – qtz, slt, ls
Proterozoic Eon 2.5 bya to 541 mya			Miette – sla, sch, grit, dol
Archean Eon 4 bya to 2.5 bya			Hearne – gn, gr

Legend

(N) Non-marine
(M) Marine
(N/M) Mixed

Carbonates
Fine clastics
Coarse clastics

Rock type

chrt chert
cgl conglomerate
col coal
dol dolomite
gn gneiss
gr granite
grit gritstone
gyp gypsum
qtz quartzite
ls limestone
pho phosphate
sch schist
sh shale
sla slate
slt siltstone
ss sandstone

Figure S1. Geologic column of the central region of the Canadian Rocky Mountains, modified from Gadd (2009). The sampling sites in this study primarily lie on Cambrian bedrock (depicted by the pickaxe). The mammoth icon was created by PizzaOtter from Noun Project (CC BY 3.0) and the remaining icons are open source stock art.

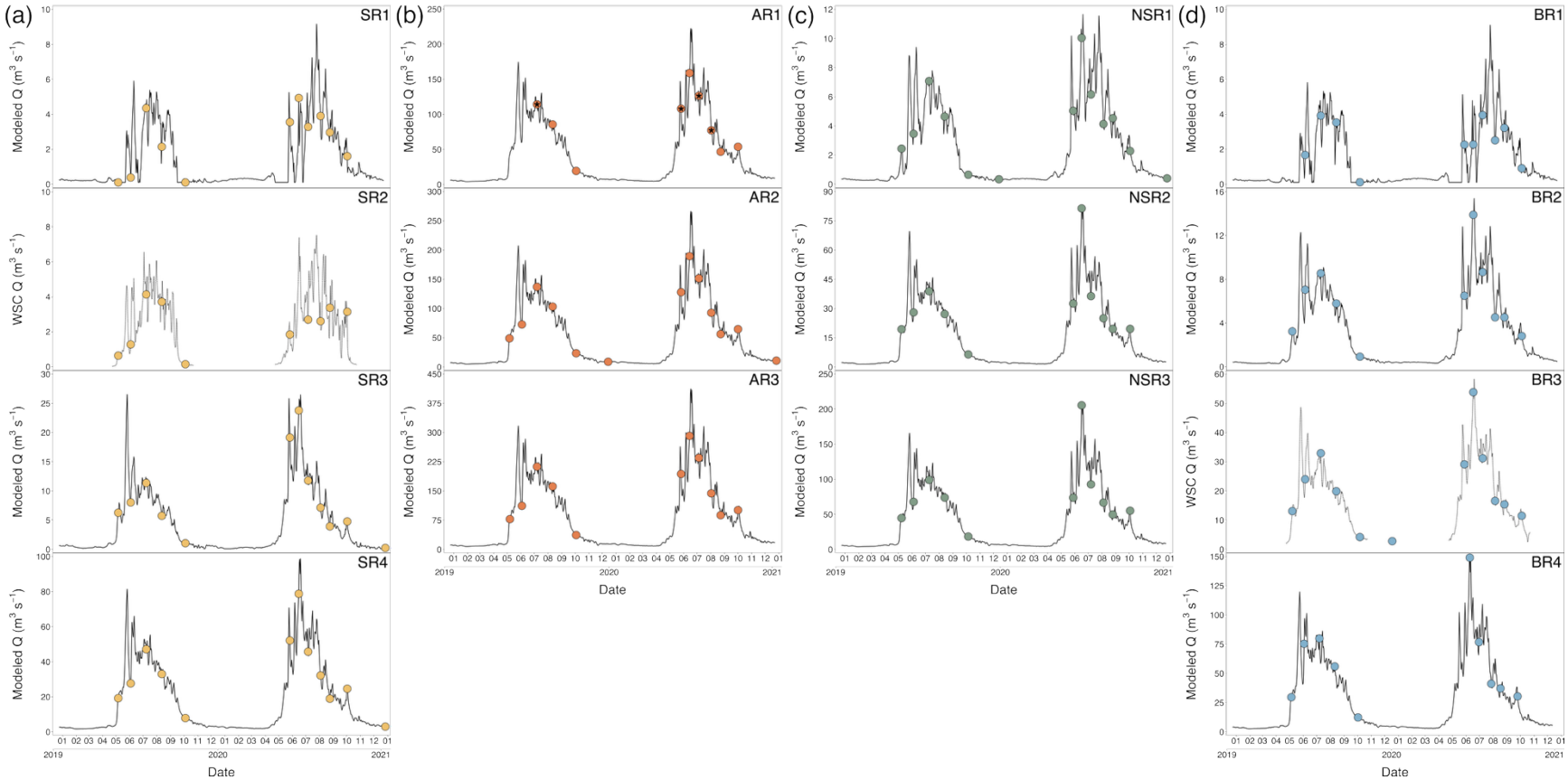

Figure S2. Modeled (solid line) and measured Water Survey of Canada (WSC; dotted line) discharge (Q; m^3 s^{-1}) and physicochemical sampling dates (colored circles) at the 14 sampling sites along the (a) Sunwapta (SR), (b) Athabasca (AR), (c) North Saskatchewan (NSR), and (d) Bow (BR) rivers for 2019 through early 2021. Stars in the orange circles for AR1 symbolize sampling dates where dissolved concentration data was eliminated from all data analyses. Please note different y-axis scales. Originally published in Serbu et al. (2023, 2024).

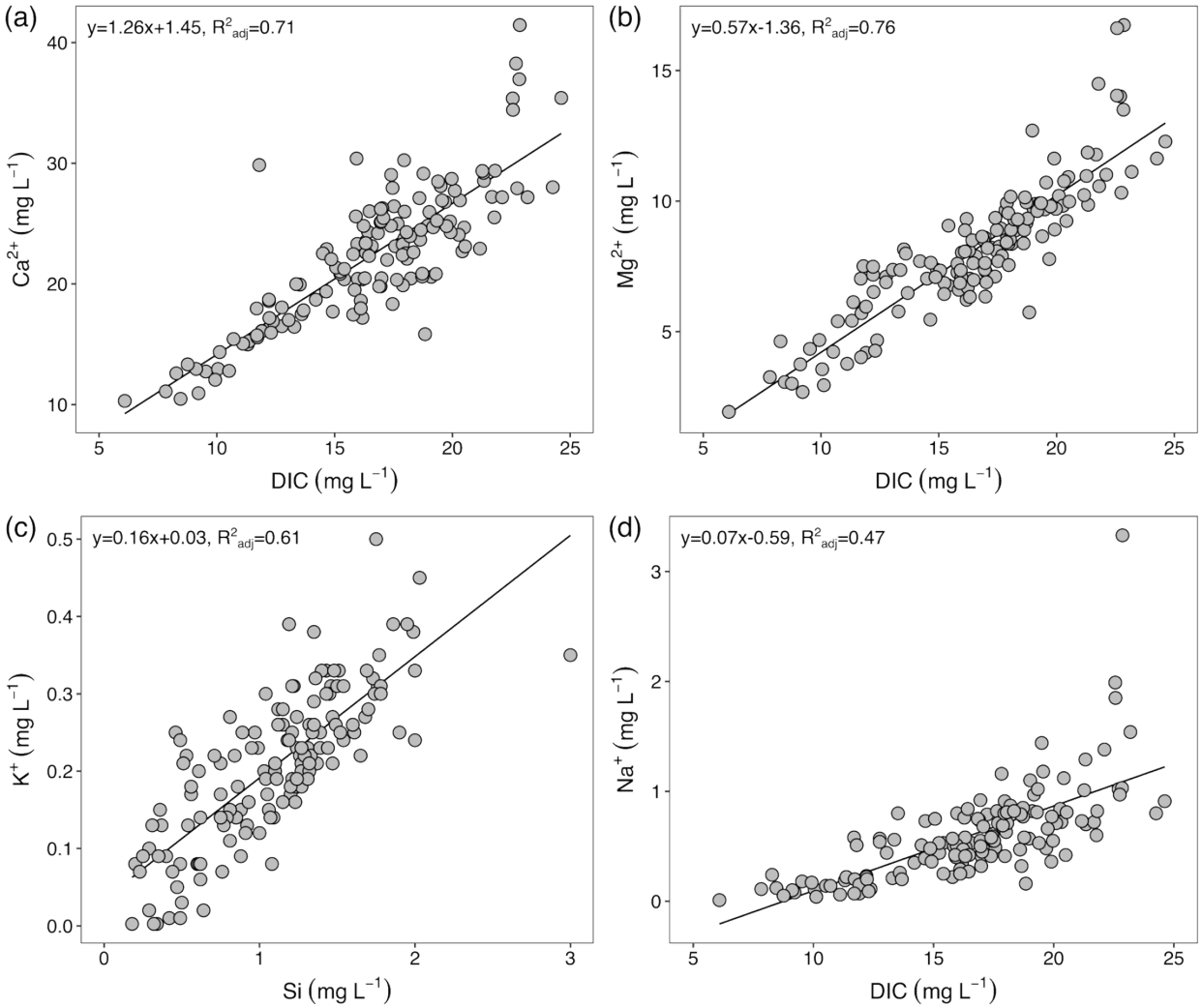

Figure S3. Linear relationships between (A) dissolved inorganic carbon (DIC) and Ca^{2+}, (B) DIC and Mg^{2+}, (C) Si and K^{+}, and (D) DIC and Na^{+}. These relationships were used to interpolate five missing cation datapoints from the first sampling trip (May 2019).

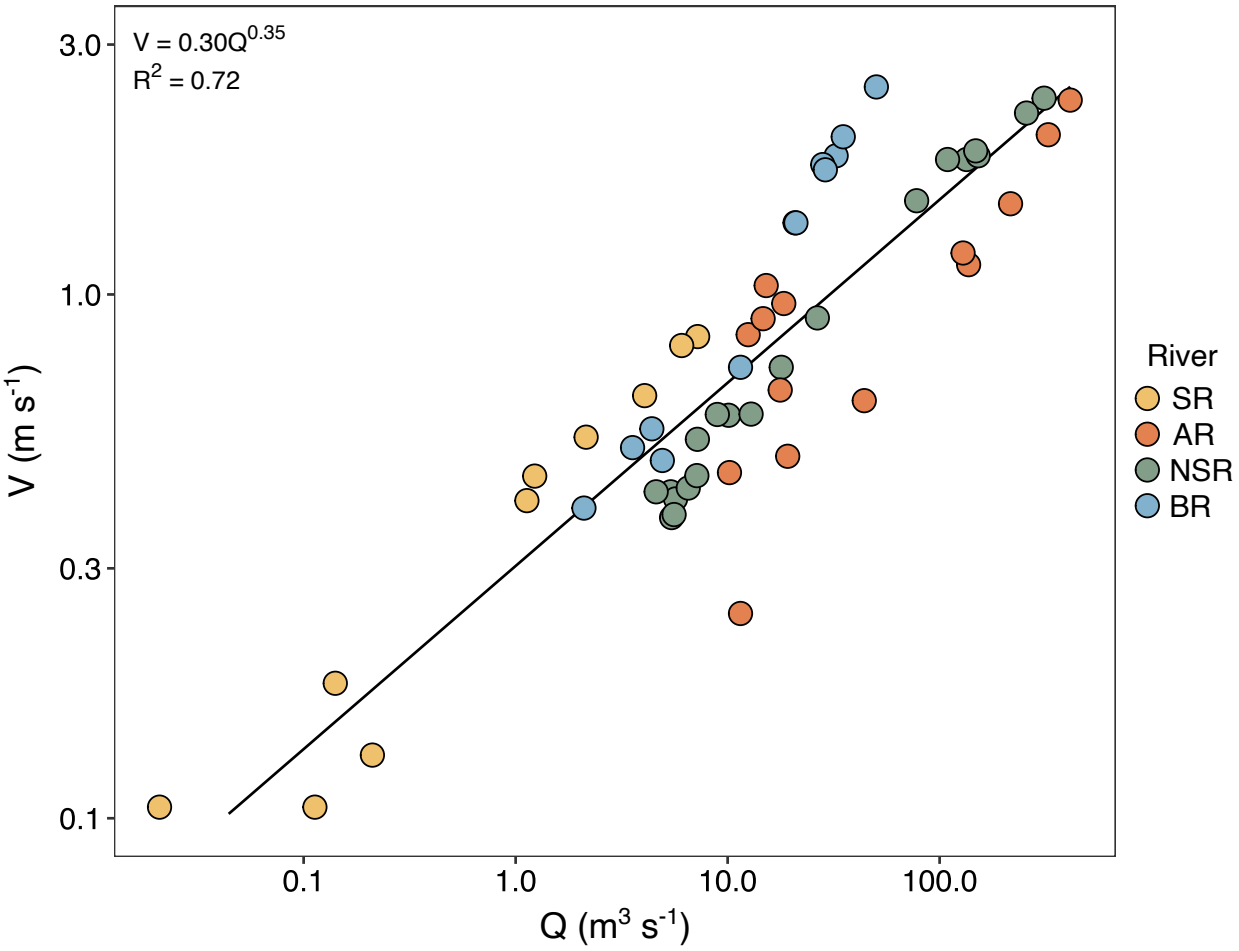

Figure S4. The power relationship between river discharge (Q) and velocity (V). Q and V were measured by the Water Survey of Canada from 2019 to 2021 at four hydrometric gauging stations along our study rivers (the Sunwapta (SR), Athabasca (AR), North Saskatchewan (NSR), and Bow (BR) rivers), described in **Table S3**. The power regression equation and coefficient of determination (R^2) for the Q-V relationship is shown in the top left of the graph.

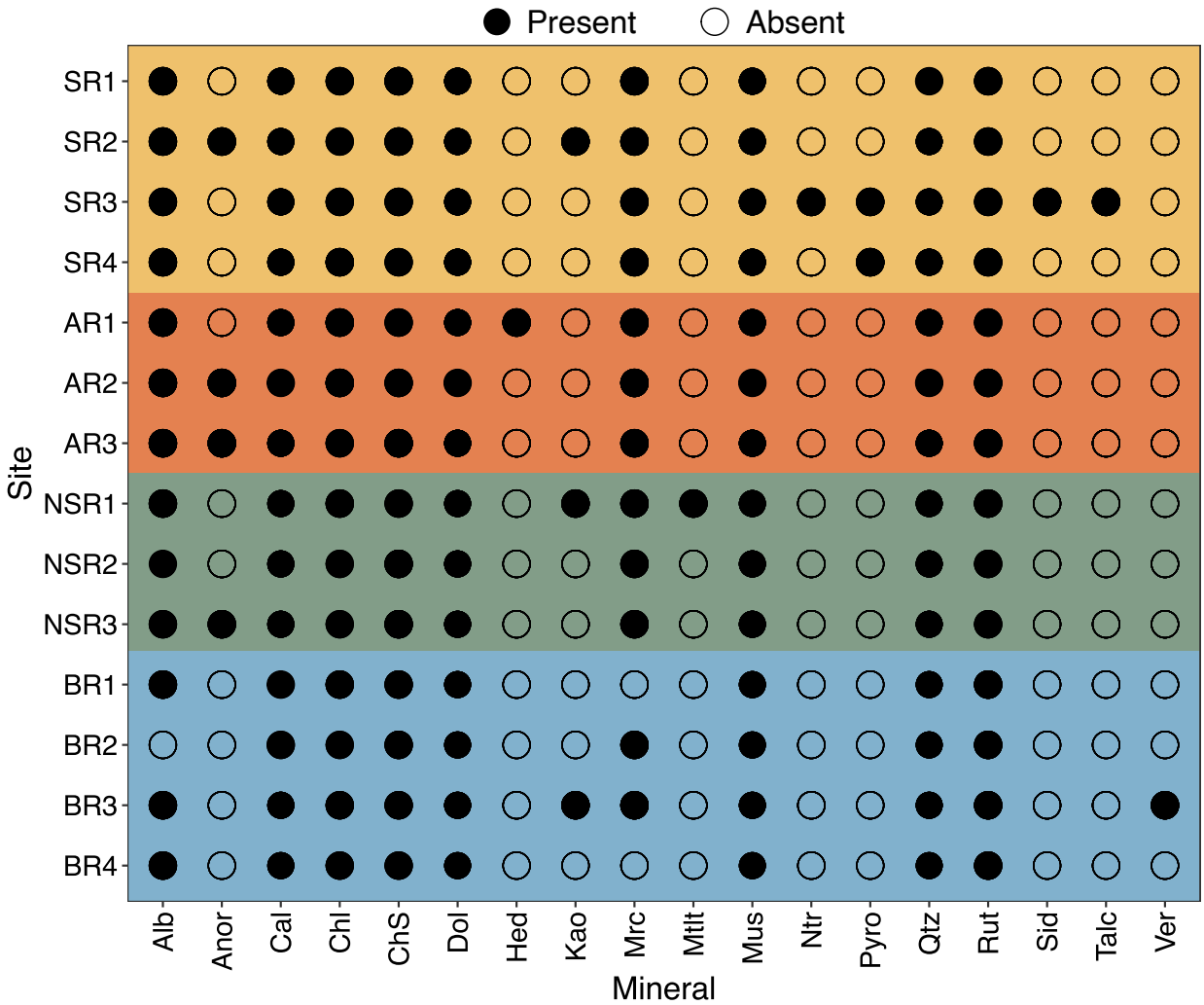

Figure S5. X-Ray Diffraction (XRD) minerology present/absent results from sampling sites along the Sunwapta (SR), Athabasca (AR), North Saskatchewan (NSR), and Bow (BR) rivers, with background colors relating to rivers. All data were combined for this figure, meaning if a mineral showed up only once at a site, it was marked as "present". Alb = Albite, Anor = Anorthite, Cal = Calcite, Chl = Clinochlore, ChS = Chlorite-Serpentine, Dol = Dolomite, Hed = Hedenbergite, Kao = Kaolinite, Mrc = Microcline, Mtlt = Montmorillonite, Mus = Muscovite, Ntr = Nontronite, Pyro = Pyrophyllite, Qtz = Quartz, Rut = Rutile, Sid = Siderotil, Talc = Talc, Ver = Vermiculite.

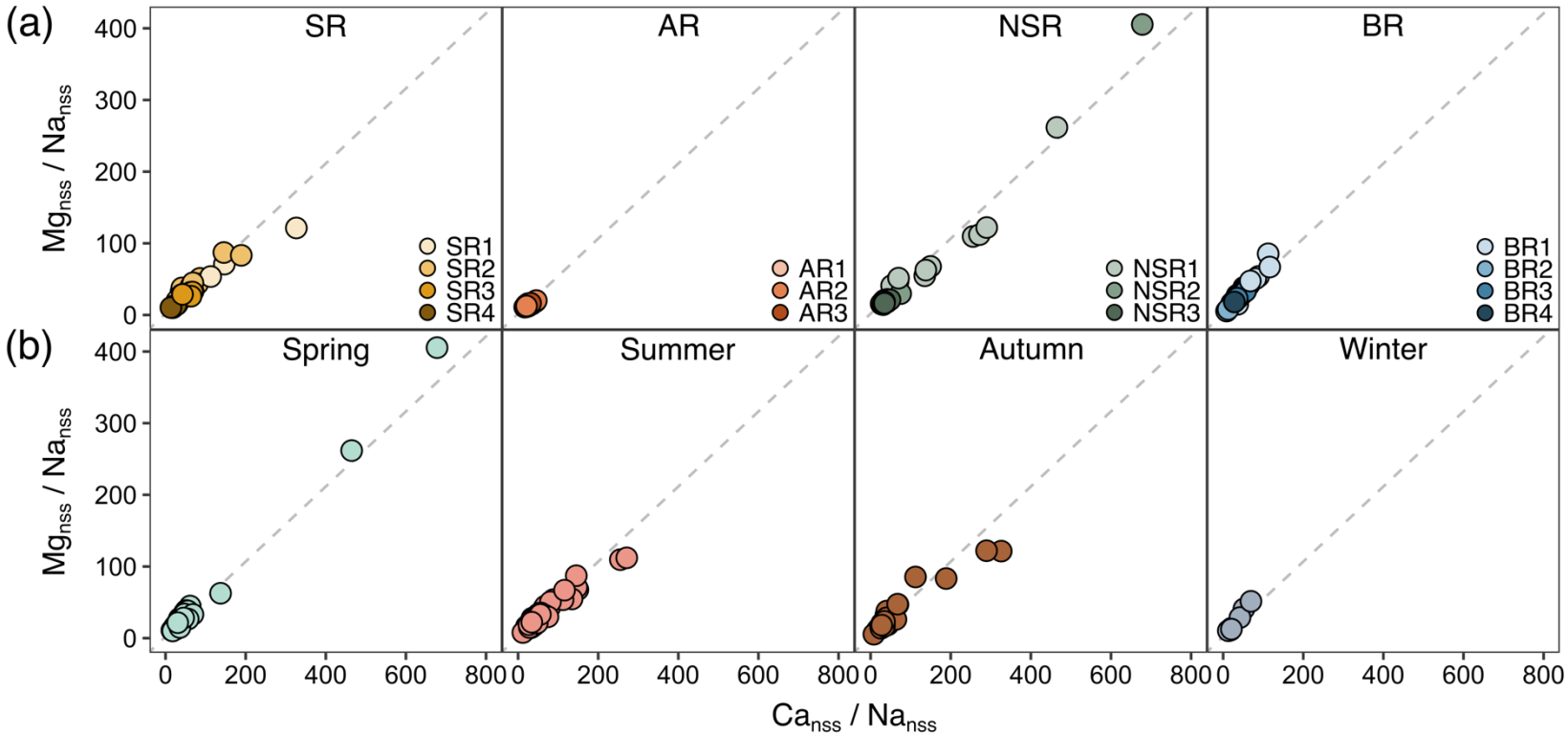

Figure S6. Mixing diagrams of non-sea salt (nss) molar Ca/Na concentrations versus molar Mg/Na concentrations by (A) river and (B) season. In panel (A), rivers are SR (Sunwapta River), AR (Athabasca River), NSR (North Saskatchewan River), and BR (Bow River), and colors are related to sampling sites. The dashed grey line is the line of best fit.

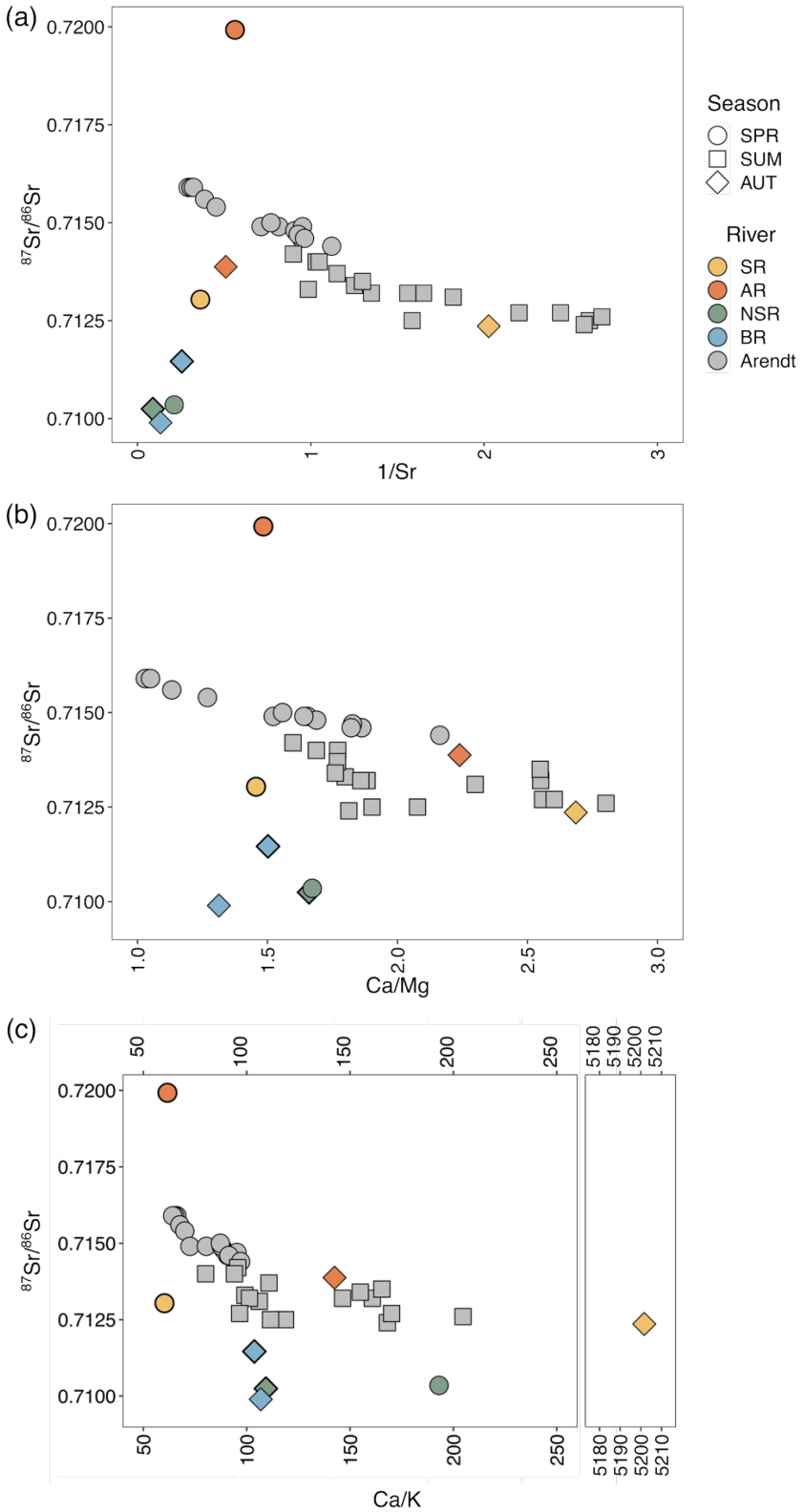

Figure S7. Molar ratios versus $^{87}Sr/^{86}Sr$, including (A) the inverse concentration of Sr (μM^{-1}), and (B) molar Ca^{2+}/Mg^{2+} and (C) molar Ca^{2+}/K^{+} ratios. Thick black outlines denote downstream sites. Grey data were collected proximal to sampling site SR1 and published in Arendt et al. (2016).

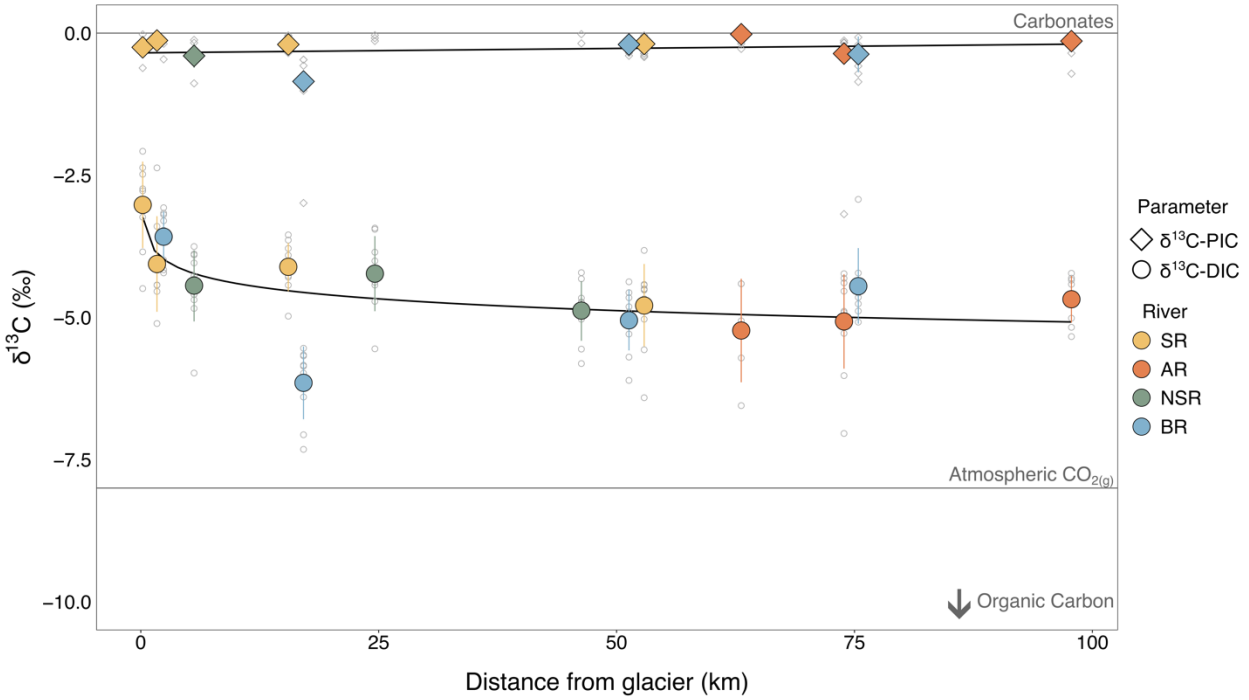

Figure S8. $\delta^{13}C$ (‰) signatures of dissolved inorganic carbon (DIC; circles) and particulate inorganic carbon (PIC; diamonds) with downriver distance from source glaciers (km) along the Sunwapta (SR), Athabasca (AR), North Saskatchewan (NSR), and Bow (BR) rivers. Colored symbols are means with the standard deviation as bars, while individual datapoints from all seasons are seen outlined in grey.

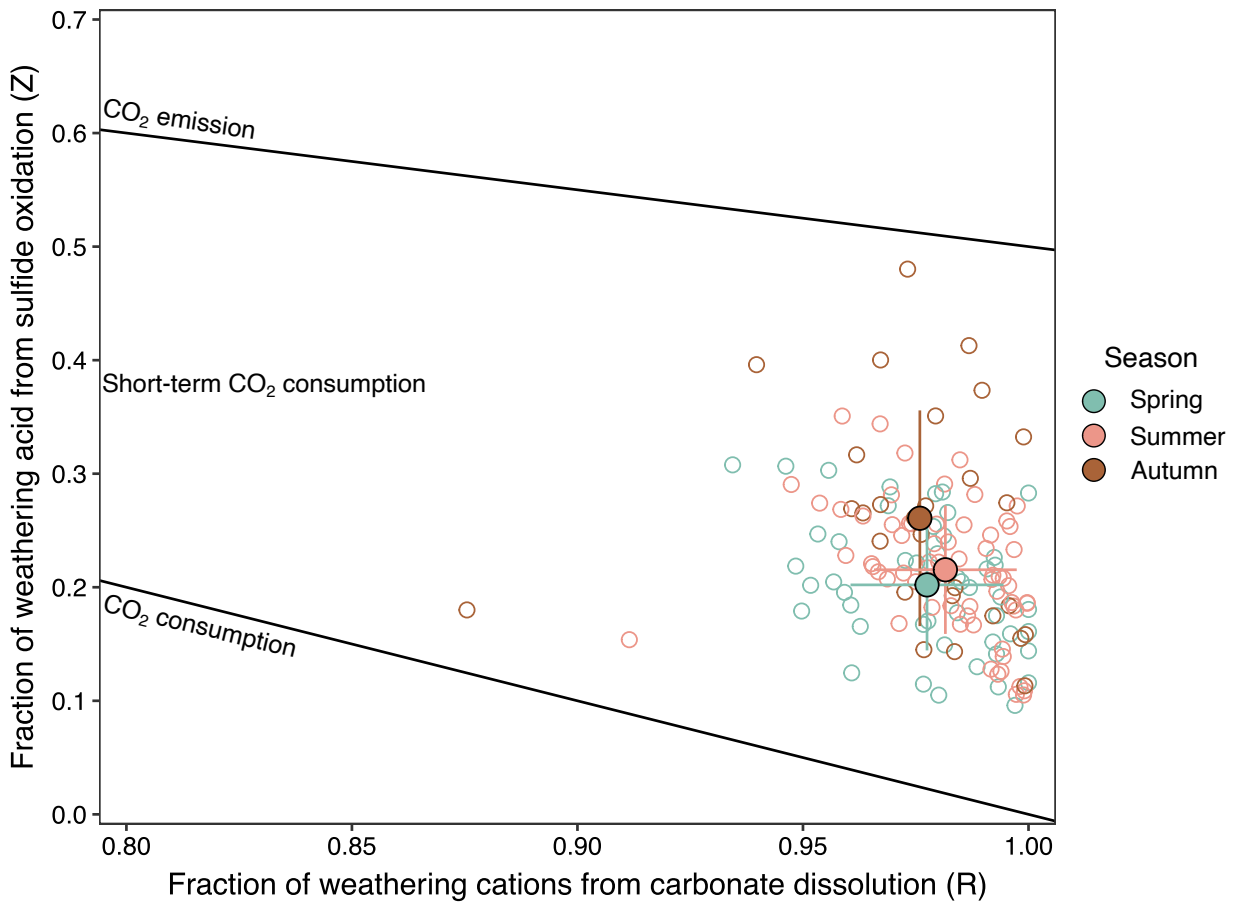

Figure S9. The fraction of weathering cations from carbonate dissolution (R) versus fraction of weathering acid from sulfide oxidation (Z) for each inversion model sample, color-coded by (A) site, (B) distance from glacier, and (C) season. Each datapoint is represented as a filled circle except in (C) where each datapoint is a hollow circle and mean seasonal data (± standard deviation) is the filled circle.

Table S1. Distance from glacier, watershed area, elevation, coordinates, and description of our 14 sampling sites along the study rivers in Jasper and Banff National Parks. Asterisked (*) sampling sites are those that have Water Survey of Canada (WSC) hydrometric gauging stations.

Site ID	Distance from glacier (km)	Watershed area (km^2)	Elevation (m)	Coordinates (DD)		Site description
				Latitude	Longitude	
Sunwapta River (SR)[1]						
SR1	0.2	22.7	2063	52.206739	-117.234767	Near Athabasca Glacier terminus
SR2*	1.7	29.3	1951	52.216950	-117.234069	Outflow of proglacial Sunwapta Lake; WSC station ID 07AA007
SR3	15.5	197.5	1580	52.310583	-117.332583	Glacial outwash plain
SR4	52.9	730.8	1396	52.532972	-117.644222	Upstream of Sunwapta Falls
Athabasca River (AR)[1]						
AR1	63.1	1635.1	1240	52.594869	-117.805439	Mt. Christie Picnic Area
AR2	73.9	1955.8	1184	52.662917	-117.881028	Upstream of Athabasca Falls
AR3	97.8	3019.9	1060	52.812056	-118.042556	At Mile Five Bridge
North Saskatchewan River (NSR)[2]						
NSR1	5.6	76.2	1682	52.169472	-117.076361	At Highway 93 bend
NSR2	24.6	616.3	1440	52.069194	-116.915250	Glacial outwash plain
NSR3	46.3	1550.7	1400	51.970556	-116.721111	At North Saskatchewan Crossing
Bow River (BR)[2]						
BR1	2.4	21.4	1996	51.661750	-116.486939	Inflow of subalpine Bow Lake
BR2	17.1	104.7	1840	51.631500	-116.335167	Outflow of wetland at Mosquito Creek Campground
BR3*	51.3	422.0	1560	51.428667	-116.189000	In Lake Louise Township; WSC station ID 05BA001
BR4	75.4	1103.9	1480	51.284950	-115.983500	Upstream of Castle Junction

[1]Jasper National Park, Alberta
[2]Banff National Park, Alberta

Table S2. Relative percent watershed area of each sampling site covered by major and minor land cover classes. Originally published in Serbu et al. (2024).

Site ID	Water[1]	Snow and ice	Rock and rubble	Exposed land	Shrubland	Grassland	Coniferous forest	Broadleaf forest	Mixed forest	Developed	Total
	%	%	%	%	%	%	%	%	%	%	%
SR1	1.1	50.7	46.8	0.0	0.0	0.0	0.0	0.0	0.0	0.0	98.6
SR2	1.5	41.8	54.2	0.0	0.2	0.1	0.3	0.0	0.0	0.8	98.9
SR3	1.0	19.1	55.3	0.0	5.7	4.7	12.8	0.2	0.1	1.1	99.8
SR4	1.5	6.6	50.2	0.0	8.4	6.8	25.1	0.4	0.1	0.8	100.0
AR1	1.9	12.2	43.2	0.1	7.6	6.4	27.3	0.6	0.2	0.4	99.9
AR2	1.9	10.8	42.8	0.0	7.7	6.4	29.0	0.7	0.3	0.4	99.9
AR3	1.9	8.4	41.2	0.0	7.4	7.4	32.0	0.8	0.3	0.5	99.9
NSR1	0.6	54.7	35.3	0.2	1.7	3.7	3.6	0.2	0.0	0.0	100.0
NSR2	1.6	19.1	40.8	0.1	7.4	5.6	24.4	0.2	0.1	0.5	99.8
NSR3	2.1	18.8	37.4	0.1	6.9	4.0	29.7	0.1	0.0	0.5	99.7
BR1	2.0	41.5	47.7	0.0	2.4	1.4	4.8	0.0	0.0	0.0	99.9
BR2	4.3	11.1	42.0	0.0	8.4	1.3	31.4	0.0	0.0	1.5	100.0
BR3	3.6	9.6	35.7	0.0	6.7	1.8	41.0	0.0	0.0	1.4	99.8
BR4	2.4	5.6	38.1	0.0	8.7	2.5	41.3	0.0	0.0	1.3	99.9

[1]Relative percent wetland cover (fen + bog + marsh + swap) was quantified separately and likely overlapped with the water land cover class. Watershed area covered by wetland at our study sites ranged from 0.0-2.1 %. Wetland cover exceeding 1.0 % were found at BR2 (2.1 %), BR3 (1.9 %), and BR4 (1.6 %).

Table S3. Water Survey of Canada (WSC) hydrometric gauging station information, including station name, station ID, watershed, watershed area, and whether discharge data was continuous or seasonal (May - October), for the nine WSC stations that were used to model discharge for our hydrometrically ungauged sampling sites (**Figure S2**) (Water Survey of Canada, 2021). Four of the gauging stations were then used to determine a relationship between measured discharge (Q) and water velocity (V) (**Figure S4**).

WSC station name (Site ID in brackets, if relevant)	Station ID	Watershed	Watershed area (km^2)	Continuous or seasonal data	Q-V model
Sunwapta River at Athabasca Glacier (SR2)	07AA007	Sunwapta/Athabasca	29.3	Seasonal	Yes
Miette River near Jasper	07AA001	Athabasca	629.0	Continuous	No
Athabasca River near Jasper	07AA002	Athabasca	3870.0	Continuous	Yes
Silverhorn Creek near the Mouth	05DA010	North Saskatchewan	21.0	Continuous	No
Mistaya River near Saskatchewan Crossing	05DA007	North Saskatchewan	248.0	Continuous	No
North Saskatchewan River at Whirlpool Point	05DA009	North Saskatchewan	1920.0	Continuous	Yes
Pipestone River near Lake Louise	05BA002	Bow	306.0	Continuous	No
Bow River at Lake Louise (BR3)	05BA001	Bow	422.0	Seasonal	Yes
Bow River at Banff	05BB001	Bow	2210.0	Continuous	No

Table S4. Dates (2019 – 2021) of river sampling trips binned into seasons for data analysis and interpretation.

Season	Sampling Dates	
	2019	2020/2021
Spring	May 14-16 June 11-13	June 3-5 June 22-25
Summer	July 15-18 August 19-22	July 13-16 August 10-13
Autumn	NA October 11-14	August 31-September 3 October 9-12
Winter	December 20-22	January 28-29 (2021)

Table S5. Median proportions and the 25th and 75th percentiles of precipitation, evaporite, carbonate, silicate, and pyrite endmembers for dissolved river Ca^{2+}, Mg^{2+}, Na^{+}, Cl^{-}, and SO_4^{2-}. Mean values of each proportion were taken from all sampling sites and seasons.

Endmember	Ca^{2+}			Mg^{2+}			Na^{+}			Cl^{-}			SO_4^{2-}		
	Median	25th Percentile	75th Percentile	Median	25th Percentile	75th Percentile	Median	25th Percentile	75th Percentile	Median	25th Percentile	75th Percentile	Median	25th Percentile	75th Percentile
Precipitation	0.0002	0.0000	0.0006	0.0022	0.0002	0.0050	0.1641	0.0166	0.3251	0.4063	0.0189	0.9894	0.0023	0.0003	0.0052
Evaporite	0.0046	0.0000	0.0383	0.0020	0.0000	0.0106	0.1965	0.0009	0.3720	0.5884	0.0048	0.9772	0.0207	0.0001	0.1454
Carbonate	0.9319	0.8374	1.0185	0.9613	0.8912	1.0216	0.2370	0.1154	0.3643	0.0000	0.0000	0.0000	0.0000	0.0000	0.0000
Silicate	0.0132	0.0052	0.0301	0.0159	0.0059	0.0364	0.3940	0.2759	0.5139	0.0000	0.0000	0.0000	0.0000	0.0000	0.0000
Pyrite	0.0000	0.0000	0.0000	0.0000	0.0000	0.0000	0.0000	0.0000	0.0000	0.0000	0.0000	0.0000	0.9779	0.8534	0.9939

Table S6. The proportion of relative total dissolved solids (TDS; mg L^{-1}) ± standard deviation from precipitation, atmosphere, evaporite, carbonate, silicate, and pyrite endmembers for each (A) sampling site, and (B) season.

A.

Site	Precipitation	Atmosphere	Evaporite	Carbonate	Silicate	Pyrite
SR1	0.13 ± 0.13	26.69 ± 7.12	0.54 ± 0.31	56.35 ± 6.76	1.48 ± 0.54	21.06 ± 6.32
SR2	1.71 ± 3.29	35.08 ± 6.90	0.50 ± 0.39	66.78 ± 15.65	2.07 ± 0.61	23.24 ± 10.53
SR3	5.01 ± 8.32	46.10 ± 8.29	0.85 ± 0.66	77.54 ± 16.84	2.84 ± 0.98	23.73 ± 17.76
SR4	4.69 ± 12.50	42.12 ± 5.57	1.53 ± 1.15	71.47 ± 12.12	3.95 ± 0.82	21.49 ± 14.24
AR1	4.87 ± 6.32	41.03 ± 5.53	0.42 ± 0.20	68.63 ± 10.88	3.29 ± 0.57	22.94 ± 12.37
AR2	6.80 ± 10.76	41.35 ± 8.71	0.63 ± 0.61	67.92 ± 15.02	3.86 ± 0.78	15.88 ± 8.62
AR3	3.26 ± 5.36	35.26 ± 5.90	0.75 ± 0.64	63.57 ± 12.93	4.01 ± 1.29	18.89 ± 12.57
NSR1	2.39 ± 4.47	33.38 ± 8.92	0.81 ± 0.68	62.93 ± 10.60	2.63 ± 1.53	21.76 ± 5.87
NSR2	12.86 ± 27.06	40.61 ± 8.83	1.25 ± 1.14	68.30 ± 15.77	3.93 ± 2.74	15.77 ± 7.19
NSR3	6.45 ± 9.69	46.04 ± 8.32	2.07 ± 1.84	74.83 ± 10.47	3.20 ± 1.08	18.47 ± 6.17
BR1	2.31 ± 4.59	36.29 ± 11.26	1.63 ± 2.25	65.74 ± 14.54	2.25 ± 0.68	19.12 ± 5.08
BR2	12.86 ± 15.78	44.60 ± 6.17	0.81 ± 1.03	70.48 ± 10.41	3.19 ± 0.40	17.53 ± 5.17
BR3	12.68 ± 19.19	43.52 ± 11.10	0.85 ± 0.91	70.14 ± 17.55	3.43 ± 0.93	17.49 ± 9.39
BR4	5.65 ± 8.57	44.75 ± 7.83	0.90 ± 0.39	75.33 ± 14.92	3.53 ± 0.95	22.96 ± 13.14

B.

Season	Precipitation	Atmosphere	Evaporite	Carbonate	Silicate	Pyrite
Spring	9.09 ± 16.33	41.91 ± 8.99	0.92 ± 0.84	70.01 ± 13.50	3.48 ± 1.19	18.19 ± 7.93
Summer	4.76 ± 10.46	36.64 ± 9.66	0.94 ± 0.99	64.08 ± 12.80	2.72 ± 0.94	18.41 ± 7.26
Autumn	3.40 ± 7.37	41.60 ± 8.07	1.27 ± 1.71	74.31 ± 14.76	3.51 ± 2.17	26.81 ± 16.23
Winter	1.59 ± 0.93	52.72 ± 9.86	0.85 ± 0.86	86.79 ± 9.72	3.36 ± 1.15	14.62 ± 2.64

Table S7. Median and the 25th and 75th percentiles of the fraction of weathering cations from carbonate dissolution (R) and fraction of weathering acid from sulfide oxidation (Z) for the MEANDIR inversion model run with ions and $\delta^{34}S\text{-}SO_4$ versus the MEANDIR inversion model run with ions only (Kemeny & Torres, 2021).

	R			Z		
	Median	25th Percentile	75th Percentile	Median	25th Percentile	75th Percentile
MEANDIR model with $^{34}S\text{-}SO_4$	0.979	0.961	0.988	0.220	0.201	0.224
MEANDIR model with ions only	0.979	0.962	0.987	0.227	0.223	0.234

References

Deuerling, K. M., Martin, J. B., Martin, E. E., & Scribner, C. A. (2018). Hydrologic exchange and chemical weathering in a proglacial watershed near Kangerlussuaq, west Greenland. *Journal of Hydrology*, *556*, 220–232. https://doi.org/10.1016/j.jhydrol.2017.11.002

Gadd, B. (2009). *Handbook of the Canadian Rockies*. Corex Press.

Gaillardet, J., Dupré, B., Louvat, P., & Allègre, C. J. (1999). Global silicate weathering and CO_2 consumption rates deduced from the chemistry of large rivers. *Chemical Geology*, *159*(1–4), 3–30. https://doi.org/10.1016/S0009-2541(99)00031-5

Kemeny, P. C., & Torres, M. A. (2021). Presentation and applications of mixing elements and dissolved isotopes in rivers (MEANDIR), a customizable MATLAB model for Monte Carlo inversion of dissolved river chemistry. *American Journal of Science*, *321*(5), 579–642. https://doi.org/10.2475/05.2021.03

Marshall, S. J., White, E. C., Demuth, M. N., Bolch, T., Wheate, R., Menounos, B., Beedle, M. J., & Shea, J. M. (2011). Glacier water resources on the eastern slopes of the Canadian Rocky Mountains. *Canadian Water Resources Journal*, *36*(2), 109–134. https://doi.org/10.4296/cwrj3602823

Marwick, T. R., Tamooh, F., Teodoru, C. R., Borges, A. V., Darchambeau, F., & Bouillon, S. (2015). The age of river-transported carbon: A global perspective. *Global Biogeochemical Cycles*, *29*(2), 122–137. https://doi.org/10.1002/2014GB004911

Millot, R., Gaillardet, J., Dupré, B., & Allègre, C. J. (2002). The global control of silicate weathering rates and the coupling with physical erosion: New insights from rivers of the Canadian Shield. *Earth and Planetary Science Letters*, *196*(1–2), 83–98. https://doi.org/10.1016/S0012-821X(01)00599-4

Muñoz, S., Jenckes, J., Ramos, E. J., Munk, L. A., & Ibarra, D. E. (2024). Hydrologic and landscape controls on rock weathering along a glacial gradient in South Central Alaska, USA. *Journal of Geophysical Research: Earth Surface*, *129*(3), e2023JF007255. https://doi.org/10.1029/2023JF007255

Serbu, J. A., St. Louis, V. L., Emmerton, C. A., Tank, S. E., Criscitiello, A. S., Silins, U., Bhatia, M. P., Cavaco, M. A., Christenson, C., Cooke, C. A., Drapeau, H. F., Enns, S. J. A., Flett, J. E., Holland, K. M., Lavallee-Whiffen, J., Ma, M., Muir, C. E., Poesch, M., & Shin, J. (2023). Physicochemical, particulate matter, temperature, and hydrological datasets collected from climate-threatened glacial river headwaters on the eastern slopes of the Canadian Rocky Mountains (2019-2021) [dataset]. *PANGAEA*. https://doi.org/10.1594/PANGAEA.963863

Serbu, J. A., St. Louis, V. L., Emmerton, C. A., Tank, S. E., Criscitiello, A. S., Silins, U., Bhatia, M. P., Cavaco, M. A., Christenson, C., Cooke, C. A., Drapeau, H. F., Enns, S. J. A., Flett, J. E., Holland, K. M., Lavallee-Whiffen, J., Ma, M., Muir, C. E., Poesch, M., & Shin, J. (2024). A comprehensive biogeochemical assessment of climate-threatened glacial river headwaters on the eastern slopes of the Canadian Rocky Mountains. *Journal of Geophysical Research: Biogeosciences*, *129*(1), e2023JG007745. https://doi.org/10.1029/2023JG007745

Spence, J., & Telmer, K. (2005). The role of sulfur in chemical weathering and atmospheric CO2 fluxes: Evidence from major ions, $\delta 13C_{DIC}$, and $\delta 34S_{SO4}$ in rivers of the Canadian Cordillera. *Geochimica et Cosmochimica Acta*, *69*(23), 5441–5458. https://doi.org/10.1016/j.gca.2005.07.011

St. Pierre, K. A., St. Louis, V. L., Schiff, S. L., Lehnherr, I., Dainard, P. G., Gardner, A. S., Aukes, P. J. K., & Sharp, M. J. (2019). Proglacial freshwaters are significant and previously unrecognized sinks of atmospheric CO_2. *Proceedings of the National Academy of Sciences*, *116*(36), 17690–17695. https://doi.org/10.1073/pnas.1904241116

Voss, B. M., Eglinton, T. I., Peucker-Ehrenbrink, B., Galy, V., Lang, S. Q., McIntyre, C., Spencer, R. G. M., Bulygina, E., Wang, Z. A., & Guay, K. A. (2023). Isotopic evidence for sources of dissolved carbon and the role of organic matter respiration in the Fraser River basin, Canada. *Biogeochemistry*, *164*(1), 207–228. https://doi.org/10.1007/s10533-022-00945-5